JACS
JOURNAL OF THE AMERICAN CHEMICAL SOCIETY
Communication
Cite This: J. Am. Chem. Soc. 2018, 140, 9051−9055
pubs.acs.org/JACS

γ-Iron Phase Stabilized at Room Temperature by Thermally Processed Graphene Oxide

Artur Khannanov,[†] Airat Kiiamov,[†,‡] Alina Valimukhametova,[†] Dmitrii A. Tayurskii,[†,‡] Felix Börrnert,[§] Ute Kaiser,[§] Siegfried Eigler,*[,∥] Farit G. Vagizov,*[,‡] and Ayrat M. Dimiev*[,†]

[†]Laboratory for Advanced Carbon Nanomaterials, Kazan Federal University, Kazan 420008, Russian Federation
[‡]Institute of Physics, Kazan Federal University, Kremlyovskaya str. 18, Kazan 420008, Russian Federation
[§]Materialwissenschaftliche Elektronenmikroskopie, Universität Ulm, Albert-Einstein-Allee 11, 89081 Ulm, Germany
[∥]Institute of Chemistry and Biochemistry, Freie Universität Berlin, Takustraße 3, 14195 Berlin, Germany

Supporting Information

ABSTRACT: Stabilizing nanoparticles on surfaces, such as graphene, is a growing field of research. Thereby, iron particle stabilization on carbon materials is attractive and finds applications in charge-storage devices, catalysis, and others. In this work, we describe the discovery of iron nanoparticles with the face-centered cubic structure that was postulated not to exist at ambient conditions. In bulk, the γ-iron phase is formed only above 917 °C, and transforms back to the thermodynamically favored α-phase upon cooling. Here, with X-ray diffraction and Mössbauer spectroscopy we unambiguously demonstrate the unexpected room-temperature stability of the γ-phase of iron in the form of the austenitic nanoparticles with low carbon content from 0.60% through 0.93%. The nanoparticles have controllable diameter range from 30 nm through 200 nm. They are stabilized by a layer of Fe/C solid solution on the surface, serving as the buffer controlling carbon content in the core, and by a few-layer graphene as an outermost shell.

Metal nanoparticles (NPs) on a structural support have gained significant attention in recent years as novel systems for new generations of catalysts, electrode materials in the energy conversion/storage devices, and similar applications. As an example, catalytic systems comprising Pd-NPs stabilized on graphene oxide (GO) or reduced graphene oxide (RGO) support demonstrated higher activity compared to the traditional bulk forms of catalysts.[1−3] GO is a 2D-nanomaterial that can be prepared on large-scale, and it is thus an appealing support for metal NPs. The solubility and solution phase processability of GO makes it possible to uniformly cover its surface with nucleation centers made from metal ions present in bulk salt solution.[4,5] Thermal processing of GO induces its decomposition, which is accompanied by CO and CO_2 formation, generating a distorted carbon lattice.[6,7] This disproportionation is exploited to reduce metal-ions to form NPs on the carbon surface. Point defects in the carbon lattice play obviously a crucial role in stopping the Ostwald ripening after NP formation.[8,9]

Several publications stress stabilization of NPs on layered carbon materials.[10−12] Among other metals, iron attracts constant attention due to its low cost and peculiar electro-magnetic and catalytic properties. While the stabilization of iron-containing NPs, assisted by the surface of graphene oxide, was demonstrated before, the stabilization of the γ-iron (γ-Fe) allotrope reflects a paradigm change. Iron-based NPs on the GO support can be produced in various ways.[13−16] However, thermal annealing of the variety of iron containing compounds in the presence of GO yields mostly iron oxides and iron carbide.[13,17−26] Only a few studies report on the formation of α-Fe along with iron oxides.[12,23−26]

Iron allotropes possess either the body-centered cubic (bcc) or the face-centered cubic (fcc) structure (Figure 1A). Up to

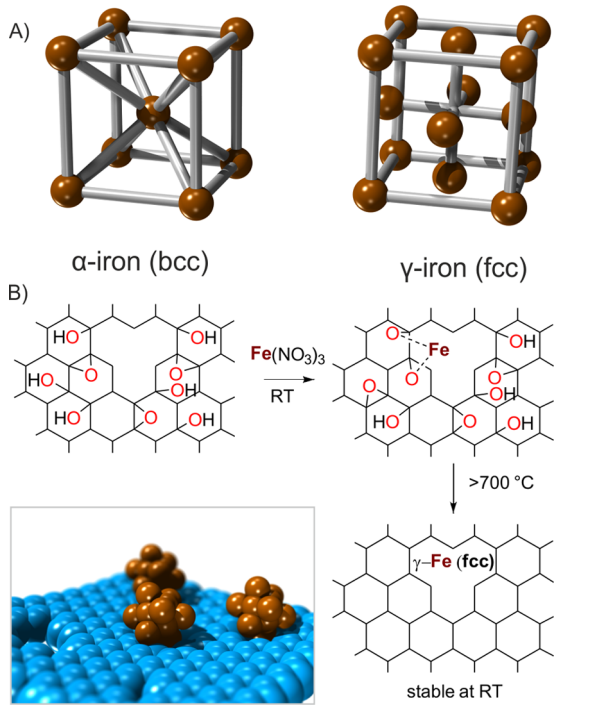

Figure 1. (A) Illustration of the structure of iron with body centered cubic and face centered cubic structure. (B) Formation mechanism of iron nanoparticles stabilized on thermally processed graphene oxide and illustration of stabilized γ-iron (face centered cubic).

Received: May 9, 2018
Published: July 9, 2018

DOI: 10.1021/jacs.8b04829
J. Am. Chem. Soc. 2018, 140, 9051−9055

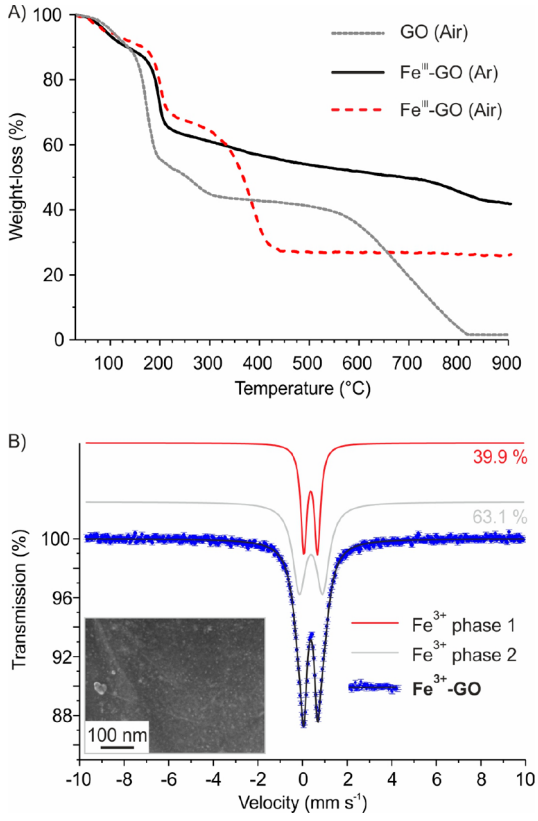

Figure 2. Fe^{3+}-GO characteristics. (A) TGA data in Ar and synthetic air, and comparison to GO. (B) Mössbauer spectrum (dotted blue line) and deconvolution into two components (red and light-gray lines). The inset of panel B is the SEM image of Fe^{3+}-GO.

769 °C, iron exists in its α-form (α-Fe), also called "metallic iron/ferrite" with the thermodynamically favored bcc lattice and ferromagnetic properties (Curie temperature, T_C, is 769 °C ≈ 1043 K). In the temperature range 769−917 °C, the β-form of iron (β-Fe) is formed, which differs from α-Fe in the magnetic properties, thus β-Fe is paramagnetic. At 917 °C, β-Fe transforms into the fcc lattice, and this allotrope is termed as γ-iron (γ-Fe) (austenite) with diamagnetic properties. According to the iron−carbon phase diagram, γ-Fe can incorporate up to 2.03% carbon. Lowering the temperature below 917 °C, carbon atoms diffuse out of the structure, and γ-Fe turns back to α-Fe. Up to now, γ-Fe could not be stabilized at room temperature, although kinetic hindrance of carbon atoms diffusion should stabilize γ-Fe.

Here, we show the stabilization of the γ-Fe allotrope NPs at room temperature on thermally processed GO (tpGO). In our two-step procedure, first Fe^{3+} is complexed with oxo-functional groups present on the surface of GO, and second γ-Fe NPs are formed upon thermal annealing. They are clearly identified as the γ-form of iron, stable at room temperature, using Mössbauer spectroscopy and X-ray diffraction (XRD). γ-Fe can be easily discriminated from α-Fe (Crystallography Open Database: COD9013415) by both methods.[27−29] Since γ-Fe was not previously reported, for reference purposes, we used the simulated XRD spectrum for the fcc lattice (Crystallography Open Database: COD9008469)[27], and the experimental Mössbauer spectrum for stainless steel, which possesses a fcc structure.[30,31]

As illustrated in Figure 1B Fe^{3+} ions covalently bind to oxo-functional groups of GO.[5] Annealing leads to GO decomposition, reduction of Fe^{3+} to Fe^0, and formation of γ-Fe NPs at sufficiently high temperature.

Table 1. Content of Different Types of Iron in Fe^{3+}-GO Samples Annealed at Different Temperatures; Based on the Mössbauer Spectroscopy Data[a]

	paramagnetic						
T (°C)	Fe^{3+}	Fe^{2+}	Fe$^{2.5+}$	Magnetically ordered Fe-oxides	α-Fe	Fe$_x$C$_y$	γ-Fe
RT	100						
300	44.5	40.0		15.5			
600	34.7	1.9		63.4			
700	31.2		30.1	4.7	25.3		8.7
800				4.4	52.1	22.5	19.5
900					35.0	15.6	49.4
950					11.8	22.1	66.1

[a]Iron phases (content in %).

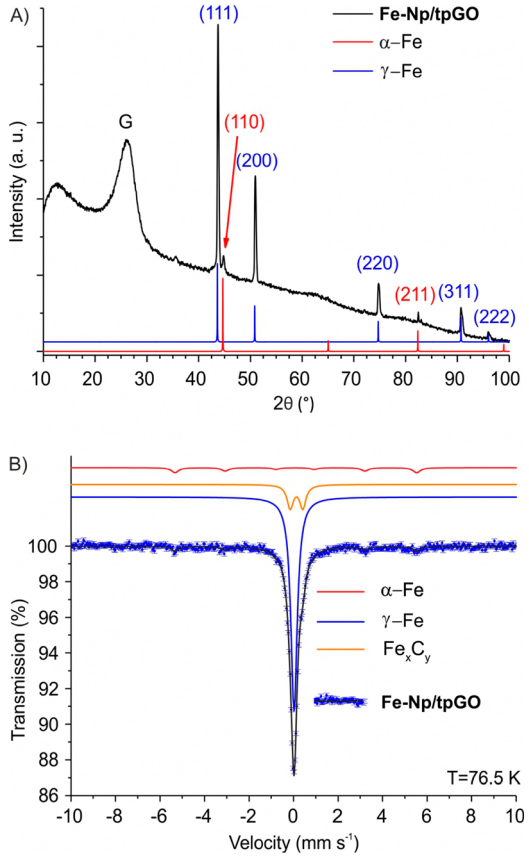

Figure 3. Characteristics of Fe^{3+}-GO annealed at 950 °C and γ-Fe formation. (A) Powder XRD pattern; the diffraction patterns for bulk forms of α-Fe and γ-Fe are given as reference. (B) Mössbauer spectrum acquired at 76.5 K.

The characteristics of Fe^{3+}-GO, formed during the solution-phase step, are presented on Figure 2. The TGA analysis in synthetic air (O_2/N_2) (Figure 2A) shows that, while GO burns to almost zero, Fe^{3+}-GO leaves 28% of the orange-colored residue, attributable, according to XRD, to iron(III) oxide. With Fe^{3+}-functionalization of GO, the thermal decomposition temperature of functional groups increases from 146−190 °C for pure GO to 170−230 °C for Fe^{3+}-GO. This observation signifies that binding of Fe^{3+} stabilizes GO functional groups against decomposition. The burning temperature of the carbon frame, contrary, shifts to lower values: from 600−800 °C to 320−400 °C, suggesting that iron clusters, forming on GO surface during the annealing, facilitate combustion of tpGO.

DOI: 10.1021/jacs.8b04829
J. Am. Chem. Soc. 2018, 140, 9051−9055

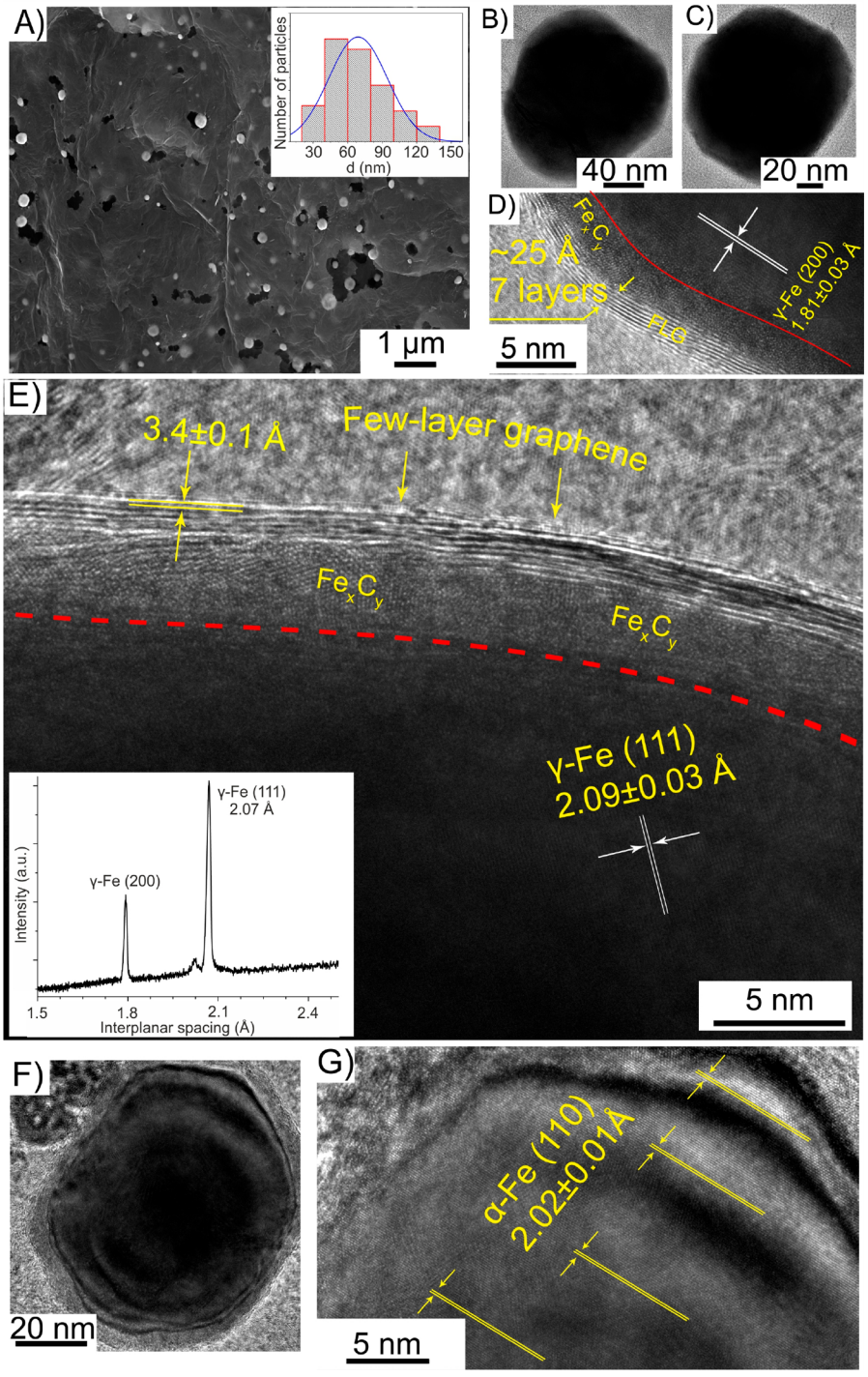

Figure 4. Characteristics of the sample annealed at 950 °C. (A) SEM image for Fe-NP/tpGO; inset: Fe-NP size distribution diagram. (B and C) TEM images of the two round-shaped Fe-NPs. (D) Magnification of the particle edge area for NP shown on panel C. (E) HRTEM image from the edge of another round-shaped Fe-NP. Inset: interplanar distances in the crystal lattice obtained from XRD. (F) TEM image of a hexagon-shaped Fe-NP. (G) Magnification of the image shown on panel F.

The Mössbauer spectrum (Figure 2B) of Fe^{3+}-GO can be deconvoluted into two components in the ratio ~2/3 (36.9%/63.1%). The isomer shift values for these components are 0.36(6) and 0.38(4) mm/s, whereas the quadruple splitting values are 0.61 and 1.11 mm/s, respectively. Thus, both components can be attributed to Fe^{3+}, either bonded to GO functional groups, or Fe^{3+}-ions bonded to each other via hydroxide ion bridges.[5] The Fourier transform infrared absorption spectroscopy (FTIR) shows conversion of ketones to carboxylates (Figure S1). Both TGA and FTIR data are consistent with our earlier work, showing the coordinate-covalent bonding between GO and Fe^{3+}.[5] No other Fe-species can be detected (discussed in SI). Consequently, only the two phases of Fe^{3+}, mentioned above, serve as the feedstock for the NP growth during the annealing step. The inset of Figure 2B shows the scanning electron micrograpy (SEM) image of Fe^{3+}-GO with shapeless light-colored features. We attribute these features to the hydroxo-clusters of Fe^{3+}, formed on the otherwise dark-colored GO surface (Figure 2B).[5]

DOI: 10.1021/jacs.8b04829
J. Am. Chem. Soc. 2018, 140, 9051−9055

Next, the Fe^{3+}-GO composite was iteratively annealed up to 900 °C, and the as-prepared samples, containing Fe^{3+}, Fe^{2+}, $Fe^{2.5+}$, Fe oxides (Fe_2O_3, Fe_3O_4) α-Fe, Fe_xC_y, and γ-Fe were analyzed by XRD and Mössbauer spectroscopy (Fe-NP/tpGO, Table 1, compare Mössbauer spectra in ESI, Figures S3−S6).

While between 300 and 600 °C, only iron oxides are formed, metallic iron is detected in the sample annealed at 700 °C. Surprisingly, the γ-Fe form was already detected (8.7%). Annealing at 900 °C leads to only α-Fe, γ-Fe, and Fe/C solid solution Fe_xC_y, with γ-Fe in majority. Interestingly, those temperatures are all below the 917 °C transition point, known for bulk iron.

The Mössbauer spectroscopy data (Table 1) are supported by the XRD data (Figure S7), showing simultaneous presence of the two allotropic forms of iron. Reflections (110), (200), and (211) at 44.67°, 65.02°, and 82.33° of 2θ angle are attributed to α-Fe. Reflections (111), (200), (220), and (311) at 43.62°, 50.81°, 74.70°, and 90.70° of 2θ angle are attributed to γ-Fe.[28] It can be seen that the signals related to α-Fe and γ-Fe, respectively, decrease and increase in intensity with increasing annealing temperature. Comparison of the obtained lattice parameters for γ-Fe with the well-established literature data for austenites suggests presence of up to 0.88% carbon (see section 3 of ESI for details). In the diffractograms, there are no signals associated with other crystalline forms of iron.

In a separate experiment, we annealed Fe^{3+}-GO at 950 °C. The XRD pattern (Figure 3A) shows that the signals related to γ-Fe heavily dominate those related to α-Fe.

The Mössbauer spectrum could be fitted by one singlet (γ-Fe), one doublet (Fe_xC_y), and one sextet for α-Fe (Figure 3B). The central narrow singlet with IS = −0.08(9) mm/s must be attributed to γ-Fe in which each iron atom is surrounded by 12 neighboring iron atoms, as in the bulk fcc lattice of γ-Fe. A solid solution of Fe_xC_y is manifested as a doublet, because of the nonequivalent surroundings of the iron atoms. This is confirmed by the shift of the signal to the region of higher velocities IS = 0.1. The content of the different forms of iron is 66.1% γ-Fe, 22.1% Fe_xC_y, and 11.8% α-Fe. Fe_xC_y and γ-Fe both have the fcc lattice structure. The lack of the Fe_xC_y signals on the XRD pattern suggests either a small-crystalline size of Fe_xC_y, or that its reflexes overlap with those for γ-Fe. Thus, formally the Fe_xC_y, phase can be considered as a part of the γ-Fe phase; when combined it constitutes 88.3% out of all the iron in the sample.

In the SEM (Figure 4A) and TEM (Figure 4B,C) images, most of the Fe-NPs appear as round-shaped multifacet nanocrystals, which consist of three distinct phases/layers. The dense crystalline core constitutes ∼90% of the NP volume; it is surrounded by a 3−5 nm layer, differing structurally from the core, and by a shell of few-layer graphene.

The crystal lattice of the main nanoparticle body is clearly visible. It is a poly crystal with crystallites of several nanometer size. The crystallites have the interplanar distance of 2.09 ± 0.03 Å, which is very close to 2.07 Å obtained for γ-Fe from the XRD data (Figure 3A, 4D,E). It is significantly distinct from the 2.02 Å, obtained for α-Fe. Thus, the analysis supports fcc of γ-Fe. Electron energy-loss spectroscopy (EELS) performed locally on the nanoparticles does not show a significant oxygen signal (Figure S11).

We assign the intermediate layer to a solid Fe/C solution with relatively high carbon content, and the formula Fe_xC_y. This is consistent with the Mössbauer data discussed above (Figure 3B, Table 1). Apparently, during annealing, carbon from tpGO diffuses into the NP and alloys with iron. The dynamic equilibrium between the core and the Fe_xC_y shell thoroughly controls the carbon content in the core needed for stabilization of γ-Fe. On the other hand, the excess of carbon diffuses out of the particle by forming graphene layers on the surface. Here the mechanism of the graphene formation is similar to the growth on copper or nickel. The few-layer graphene provides additional protection. This complex, but self-forming structure results in kinetic hindrance for converting γ-Fe into the thermodynamically favorable α-Fe.

In minority, hexagon-shaped single crystal NPs were detected (Figure 3F,G) with interplanar distance of 2.02 ± 0.01 Å, which can be assigned to pure α-Fe, thus existing separately from the γ-phase.

In an additional experiment we obtained Fe-NPs by annealing Fe^{3+}-GO at 800 °C for 8 h (SI Figure S12, S13). The content of the different iron phases (64.1% γ-Fe, 16.7% α-Fe, 19.2% Fe_xC_y) was similar to the sample obtained by annealing at 950 °C, However, the particle size was significantly smaller, 30−55 nm. Further reference experiments demonstrate the unique role of GO in this process, and are discussed in section 5 of the SI.

To conclude, impregnation of GO with $Fe(NO_3)_3$ and subsequent annealing yields NPs of γ-Fe. The γ-Fe phase is stabilized in the form of NPs with complex structure. The self-controlled formation of a thin layer of the Fe/C solid solution on the surface serves as the buffer, controlling carbon content in the NP core. We further conclude that GO with its vacancy defects in the lattice is a unique material that surprisingly allows the preparation and stabilization of γ-Fe-NPs. GO plays the role of the nucleating site, the reducing agent, the carbon source, and the stabilizer for as formed γ-Fe-NPs. The here presented discovery of γ-Fe will allow the study of the properties of γ-Fe-NPs, including catalytic activity or materials preparation.

■ ASSOCIATED CONTENT

Supporting Information

The Supporting Information is available free of charge on the ACS Publications website at DOI: 10.1021/jacs.8b04829.

Synthetic methods; FTIR spectra; XRD spectra; Mössbauer spectra; photographs of materials; TEM image and electron energy-loss spectroscopy (PDF)

■ AUTHOR INFORMATION

Corresponding Authors

*AMDimiev@kpfu.ru
*vagizovf@gmail.com
*siegfried.eigler@fu-berlin.de

ORCID

Siegfried Eigler: 0000-0002-0536-8256
Ayrat M. Dimiev: 0000-0001-7497-1211

Notes

The authors declare no competing financial interest.

■ ACKNOWLEDGMENTS

This research was conducted with support of the Russian Science Foundation, Grant # 16-13-10291. The SEM images end electron diffraction were acquired using the equipment of the Interdisciplinary Center for Analytical Microscopy, Kazan Federal University. S.E. is gratefully acknowledges funding

DOI: 10.1021/jacs.8b04829
J. Am. Chem. Soc. 2018, 140, 9051−9055

from the Deutsche Forschungsgemeinschaft (DFG, German Research Foundation), 392444269.

REFERENCES

(1) Scheuermann, G. M.; Rumi, L.; Steurer, P.; Bannwarth, W.; Mülhaupt, R. *J. Am. Chem. Soc.* **2009**, *131*, 8262.
(2) Pyun, J. *Angew. Chem., Int. Ed.* **2011**, *50*, 46.
(3) Lightcap, I. V.; Kosel, T. H.; Kamat, P. V. *Nano Lett.* **2010**, *10*, 577.
(4) Dimiev, A. M.; Eigler, S. *Graphene Oxide: Fundamentals and Applications*; John Wiley & Sons, Ltd.: Chichester, 2016.
(5) Amirov, R. R.; Shayimova, J.; Nasirova, Z.; Dimiev, A. M. *Carbon* **2017**, *116*, 356.
(6) Grote, F.; Gruber, C.; Börrnert, F.; Kaiser, U.; Eigler, S. *Angew. Chem., Int. Ed.* **2017**, *56*, 9222.
(7) Dimiev, A. M.; Eigler, S. *Graphene Oxide: Fundamentals and Applications*; John Wiley & Sons, Ltd.: Chichester, 2016; Chapter 6.
(8) Chen, Y.; Song, B.; Tang, X.; Lu, L.; Xue, J. *J. Mater. Chem.* **2012**, *22*, 17656.
(9) Chen, X.; Wu, G.; Chen, J.; Chen, X.; Xie, Z.; Wang, X. *J. Am. Chem. Soc.* **2011**, *133*, 3693.
(10) Gao, Y.; Ma, D.; Hu, G.; Zhai, P.; Bao, X.; Zhu, B.; Zhang, B.; Su, D. S. *Angew. Chem., Int. Ed.* **2011**, *50*, 10236.
(11) Kou, R.; Shao, Y.; Mei, D.; Nie, Z.; Wang, D.; Wang, C.; Viswanathan, V. V.; Park, S.; Aksay, I. A.; Lin, Y.; Wang, Y.; Liu, J. *J. Am. Chem. Soc.* **2011**, *133*, 2541.
(12) Tucek, J.; Sofer, Z.; Bousa, D.; Pumera, M.; Hola, K.; Mala, A.; Polakova, K.; Havrdova, M.; Cepe, K.; Tomanec, O.; Zboril, R. *Nat. Commun.* **2016**, *7*, 12879.
(13) Zhang, L.; Yu, X.; Hu, H.; Li, Y.; Wu, M.; Wang, Z.; Li, G.; Sun, Z.; Chen, C. *Sci. Rep.* **2015**, *5*, 9298.
(14) Gan, N.; Zhang, J.; Lin, S.; Long, N.; Li, T.; Cao, Y. *Materials* **2014**, *7*, 6028.
(15) Li, L.; Zeng, C.; Ai, L.; Jiang, J. *J. Alloys Compd.* **2015**, *639*, 470.
(16) Liu, C.; Yan, H.; Lv, Q.; Li, S.; Niu, S. *Carbon* **2016**, *102*, 145.
(17) Torres Galvis, H. M.; Bitter, J. H.; Khare, C. B.; Ruitenbeek, M.; Dugulan, A. I.; de Jong, K. P. *Science* **2012**, *335*, 835.
(18) Bi, X.-X.; Ganguly, B.; Huffman, G. P.; Huggins, F. E.; Endo, M.; Eklund, P. C. *J. Mater. Res.* **1993**, *8*, 1666.
(19) Huang, X.; Niu, Y.; Hu, W. *Colloids Surf., A* **2017**, *518*, 145.
(20) Niu, Y.; Huang, X.; Hu, W. *J. Power Sources* **2016**, *332*, 305.
(21) Lv, X. S.; Qiu, Y.; Wang, Z. Y.; Jiang, G. M.; Chen, Y. T.; Xu, X. H.; Hurt, R. H. *Environ. Sci.: Nano* **2016**, *3*, 1215.
(22) Jia, X.; Lian, D.; Shi, B.; Dai, R.; Li, C.; Wu, X. *J. Mater. Sci.: Mater. Electron.* **2017**, *28*, 12070.
(23) Wang, Y.; He, Q.; Qu, H.; Zhang, X.; Guo, J.; Zhu, J.; Zhao, G.; Colorado, H. A.; Yu, J.; Sun, L.; Bhana, S.; Khan, M. A.; Huang, X.; Young, D. P.; Wang, H.; Wang, X.; Wei, S.; Guo, Z. *J. Mater. Chem. C* **2014**, *2*, 9478.
(24) Guo, Y.; Zeng, Z.; Li, Y.; Huang, Z.; Cui, Y. *Catal. Today* **2018**, *307*, 12.
(25) Awadallah, A. E.; Aboul-Enein, A. A.; Kandil, U. F.; Taha, M. R. *Mater. Chem. Phys.* **2017**, *191*, 75.
(26) Schettino, M. A., Jr; Cunha, A. G.; Nunes, E.; Passamani, E. C.; Freitas, J. C. C.; Emmerich, F. G.; Morigaki, M. K. *J. Nanopart. Res.* **2016**, *18*, 90.
(27) Gražulis, S.; Daskevic, A.; Merkys, A.; Chateigner, D.; Lutterotti, L.; Quiros, M.; Serebryanaya, N. R.; Moeck, P.; Downs, R. T.; Le Bail, A. *Nucleic Acids Res.* **2012**, *40*, D420.
(28) Kraus, W.; Nolze, G. *J. Appl. Crystallogr.* **1996**, *29*, 301.
(29) Preston, R. S.; Hanna, S. S.; Heberle, J. *Phys. Rev.* **1962**, *128*, 2207.
(30) Long, G. J. *Mössbauer Spectroscopy Applied to Inorganic Chemistry*; Springer US: New York, 1984.
(31) Mashlan, M.; Miglierini, M.; Schaaf, P. *Material Research in Atomic Scale by Mössbauer Spectroscopy*; Springer: Amsterdam, 2003.

DOI: 10.1021/jacs.8b04829
J. Am. Chem. Soc. 2018, 140, 9051−9055